Connection between water's dynamical and structural properties: Insights from ab initio simulations

Cecilia Herrero[a] , Michela Pauletti[b], Gabriele Tocci[b] , Marcella Iannuzzi[b] , and Laurent Joly[a,c,1]

Among all fluids, water has always been of special concern for scientists from a wide variety of research fields because of its rich behavior. In particular, some questions remain unanswered today regarding the temperature dependence of bulk and interfacial transport properties of supercooled and liquid water, for example, regarding the fundamentals of the violation of the Stokes–Einstein relation in the supercooled regime, or the subtle relation between structure and dynamical properties. We have studied the temperature dependence of the bulk transport properties from ab initio molecular dynamics based on density functional theory, down to the supercooled regime. We determined, from a selection of functionals, that the SCAN (strongly constrained and appropriately normed) functional best describes the experimental viscosity and self-diffusion coefficient, although we found disagreements at lower temperatures. For a limited set of temperatures, we also explored the role of nuclear quantum effects on water dynamics using ab initio molecular dynamics that was accelerated by a recently introduced machine learning approach. We then investigated the molecular mechanisms underlying the different functionals' performance and assessed the validity of the Stokes–Einstein relation. We also explored the connection between structural properties and transport coefficients, verifying the validity of the excess entropy scaling relations for all functionals. These results pave the way for the prediction of the transport coefficients from the radial distribution function, thus helping to develop better functionals. In this respect, these results indicate the importance of describing the long-range features of the radial distribution function.

water | supercooled | structure–dynamics relationship | ab initio

Water is a ubiquitous liquid, essential for life on Earth, and therefore constitutes one of the most important chemical substances. Despite the apparent simplicity of its chemical formula, water is a complex liquid that, after much effort, still evades our complete understanding at the molecular level (1). Because of its critical relevance to energy harvesting and water purification, several efforts have been made to obtain molecular insights on water behavior under different thermodynamic conditions. Water molecular interactions arise from a balance between van der Waals and hydrogen-bonding forces (2, 3); thus a complete description exclusively from classical force field (FF) simulations may hinder some critical mechanisms. Ab initio molecular dynamics (AIMD), where interatomic forces are computed from the electronic structure, may play a key role in understanding some important physical processes for bulk and confined water (4–7) such as, for instance, the controversial liquid–liquid critical point (8).

A very efficient approach to determine the electronic structure is density functional theory (DFT), based on a formulation of the many-body problem in terms of a functional of the electron density. So far, however, many widely used approximations for the exchange-correlation functional do not provide a sufficiently accurate description of many water properties (9, 10). The main challenge of semilocal and hybrid density functional approximations in predicting the structure and energetics of water lies in their description of dispersion and exchange-overlap interactions (10, 11). Additionally, nuclear quantum effects (NQEs) play an important role in determining water structure (12–15): While, on the one hand, NQEs tend to strengthen the hydrogen bond, on the other hand, competing effects due to the spread of the protons in the normal direction tend to weaken it. Although NQEs can be modeled via ab initio path integral molecular dynamics (PIMD), accounting for this subtle competition adds an additional level of complexity (12). Despite recent advances in describing water structure and thermodynamic properties (16, 17), predicting transport properties from first principles represents a further challenge (18–20). Although the temperature evolution of the diffusion coefficient and of the shear viscosity has been extensively investigated with FF simulations (21–28), limited work has been dedicated to this question using ab initio methods (3, 8, 29, 30). A clearer picture of the molecular mechanisms controlling water viscosity

Significance

First-principles calculations, which explicitly account for the electronic structure of matter, can shed light on the molecular structure and dynamics of water in its supercooled state. In this work, we use density functional theory, which relies on a functional to describe electronic exchange and correlations, to evaluate which functional best describes the temperature evolution of bulk water transport coefficients. We also assess the validity of the Stokes–Einstein relation for all the functionals in the temperature range studied, and explore the link between structure and dynamics. Based on these results, we show how transport coefficients can be computed from structural descriptors, which require shorter simulation times to converge, and we point toward strategies to develop better functionals.

and diffusion is needed, especially in the supercooled regime (31, 32), where water viscoelasticity is poorly understood (33–35) and the validity of the Stokes–Einstein (SE) relation at low temperatures remains an open question (24, 36–40).

Water dynamics is also crucial in the field of nanofluidics (41), where, in particular, the performance can be boosted by liquid–solid slip, arising from a competition between bulk liquid viscosity and interfacial friction (42–45). Further, reaching clearer insights into the molecular properties controlling water dynamics would enable the determination of a relationship between the structural correlations and molecular transport. Establishing such a thermodynamic link between structure and dynamics would also be instrumental to improve the description of water via DFT.

Such a connection has already been explored in the literature via, for example, free-volume models (46, 47), relationships between $g(r)$ and glass transition temperature (48), and the proposition of different structural descriptors (49–51), among which the entropy excess scaling, already employed for AIMD simulations of liquid metals (52) or water (53), stands out (54–56). The excess of entropy, which can be decomposed in terms of the N-body radial distribution functions (57), has been shown to exhibit an exponential relation to the diffusion coefficient for multiple systems (58, 59). In particular, for glass-forming liquids such as supercooled binary mixtures and water, the approximation of the entropy excess by its two-body contribution (related to an integral of a function of $g(r)$) has been shown to work well for a broad range of temperatures (56, 60–63). One of the main limitations for AIMD is its great need of resources as compared to its classical counterpart. Nevertheless, if the link between dynamics and structure is established, one would be able to predict the transport coefficients from structural properties, which require shorter simulation times to converge (64). Besides this, entropy excess scaling has also been used as a tool to bring insights into the molecular mechanisms underlying the SE relation (63).

In this report, we determine, from a selection of density functionals commonly used to characterize water (10, 11, 65), which one better describes the temperature dependence of the water viscosity and self-diffusion coefficient in its liquid and supercooled state, in comparison with FF simulations using the TIP4P/2005 water model (66). From these results, we proceed to explore the SE relation for the different functionals. Additionally, we explore the connection between structural properties and the transport coefficients for all the functionals proposed via the two-body entropy parameter, presenting this physical descriptor as a path to develop better functionals and better compare with experimental results. We used AIMD simulations, describing the electronic structure within DFT, in the NVT (fixed number of particles, volume, and temperature) ensemble to determine hydrodynamic bulk transport coefficients of three different density functionals: PBE (Perdew–Burke–Ernzerhof) (67) with Grimme's D3 corrections (68, 69) (namely PBE-D3), optB88-vdW (70, 71), and SCAN (strongly constrained and appropriately normed) (72). While describing the electronic structure with the SCAN functional, we also included NQEs by performing PIMD simulations for a limited set of temperatures, using a recently introduced machine learning approach to accelerate the calculation of the electronic structure problem (73). Further simulation details can be found in *Materials and Methods*.

Results and Discussion

We display, in Fig. 1A (dashed lines), the temperature evolution of the shear viscosity, determined from the long-time plateau of the Green–Kubo integral, η_{GK} (Eq. **8** in *Materials and Methods*), for
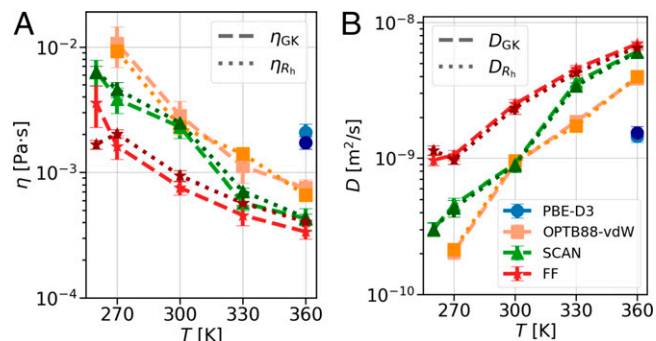

Fig. 1. Temperature evolution for different functionals of (*A*) shear viscosity and (*B*) diffusion coefficient. Good agreement is found between the results obtained in terms of the hydrodynamic radius (dotted lines) and using the Green–Kubo relation (dashed lines), implying all the functionals verify the SE relation with the same hydrodynamic radius $R_{\mathrm{h}} = 1$ Å (see text for detail).

the different functionals. No plateau was observed for PBE-D3 at $T < 360$ K and optB88-vdW at $T = 260$ K. To benchmark the results, the same procedure was carried out for FF simulations with the TIP4P/2005 water model (66), which provides an excellent description of experimental results for both viscosity and diffusion coefficient (23, 45, 74). In Fig. 1A, one can see that the viscosity obtained from the SCAN functional is in better agreement with FF at 330 and 360 K, although, between 260 and 300 K, it overestimates the viscosity by more than a factor of 1.7. With regard to PBE-D3 and optB88-vdW, one can observe that both functionals overestimate η_{GK}. Overall, all functionals fail at describing the temperature evolution of the shear viscosity.

The diffusion coefficient D_{PBC} was determined from the slope of the mean-squared displacement in the diffusive regime (*SI Appendix*). In practice, because of hydrodynamic interactions between the periodic image boxes, a finite-size correction for the diffusion coefficient has to be introduced (25, 74, 75). For a cubic simulation box of size L_{box} with periodic boundary conditions,

$$D_{\mathrm{GK}} = D_{\mathrm{PBC}} + 2.837 \frac{k_{\mathrm{B}} T}{6\pi \eta_{\mathrm{GK}} L_{\mathrm{box}}}, \qquad [1]$$

with k_{B} as the Boltzmann constant and T as the temperature. We denoted D_{GK} as the diffusion coefficient obtained through Eq. **1** because we used η_{GK} in it. D_{PBC} could not be determined within our simulation times for PBE-D3 at $T < 360$ K and optB88-vdW at $T = 260$ K because the system did not enter in the diffusive regime. This result is consistent with the absence of a plateau for η_{GK}. The corrected diffusion coefficient D_{GK} results are displayed in Fig. 1B (dashed lines). In analogy to η_{GK}, one observes, in this figure, that SCAN is the functional that better describes water diffusion coefficient at high temperatures, although it fails at low T.

Generally, viscosity η and diffusion D are related through the SE relation,

$$D = \frac{k_{\mathrm{B}} T}{6\pi \eta R_{\mathrm{h}}}, \qquad [2]$$

with R_{h} as the effective hydrodynamic radius of the molecules (76). Even though the failure of this relation is well known at low temperatures (24, 36–40), it still remains valid for a broad range of temperatures. We verified this statement by computing R_{h} for FF simulations, obtaining constant $R_{\mathrm{h}} \sim 1$ Å for the range of temperatures considered in the present study (*SI Appendix*).

Taking into account D size correction Eq. **1** and SE relation Eq. **2**, one can relate the viscosity to D_{PBC} and to the hydrodynamic radius,

$$\eta_{R_{\rm h}} = \frac{k_{\rm B}\,T}{6\pi D_{\rm PBC}} \left(\frac{1}{R_{\rm h}} - \frac{2.837}{L_{\rm box}} \right). \qquad [3]$$

In the same way, one can also determine a relation for $D_{R_{\rm h}}$ independent of η from Eqs. **1** and **2**,

$$D_{R_{\rm h}} = \frac{D_{\rm PBC}}{1 - \frac{2.837 R_{\rm h}}{L_{\rm box}}}. \qquad [4]$$

Therefore, viscosity and diffusion can be determined exclusively from the slope of the mean-squared displacement at long times by imposing the hydrodynamic radius $R_{\rm h}$. In order to test the applicability of this prediction, in Fig. 1, we display the results for $\eta_{R_{\rm h}}$ from Eq. **3** and $D_{R_{\rm h}}$ from Eq. **4** by imposing $R_{\rm h} = 1$ Å (a value in agreement with the FF measures; *SI Appendix*). In Fig. 1, one can see a good match between the Green–Kubo and the hydrodynamic radius measures for both transport coefficients and for all the functionals considered, meaning that, although all the functionals fail in predicting viscosity and diffusion temperature dependence, all of them verify the SE relation with the same constant value of $R_{\rm h}$. The validity of the SE relation indicates that the simulated systems are in the liquid or supercooled liquid state. Indeed, the SE relation is based on Einstein relation between diffusion and mobility, and on a Stokes calculation for the viscous drag force on a moving particle. The Einstein relation is a property of systems at equilibrium, so it should be valid in the liquid state (stable equilibrium), but also in the supercooled liquid state (metastable equilibrium). Stokes calculation assumes that the fluid is purely viscous, and that the viscosity is local and homogeneous; these assumptions are expected to fail when approaching the glass transition, due to viscoelasticity and dynamical heterogeneities (38, 77). As a side note, when we wrote the SE relation, we used the common mapping of the Stokes drag to that of an equivalent no-slip sphere, so that the drag force writes $F = 6\pi\eta R_h U$ (with U as the particle velocity). Although it is a less common choice, for a single molecule, one could rather map the Stokes drag to that of a perfect-slip sphere: $F = 4\pi\eta R_h^{\rm slip} U$, so that $R_h^{\rm slip} = (3/2)R_h$. The corresponding hydrodynamic diameter would then be $d_h^{\rm slip} = 3R_h \approx 3$ Å, a value similar to the Van der Waals diameter of a water molecule.

Having determined the transport properties for the different functionals, we proceed to explore their connection with the structure of water, given by the radial distribution function, $g(r)$. Specifically, we computed the structural descriptor s_2 (two-body excess entropy; *SI Appendix*), given by the integral (57),

$$\frac{s_2}{k_{\rm B}} = -2\pi n \int_0^\infty r^2 \left(g(r) \ln g(r) - g(r) + 1 \right)\, {\rm d}r, \qquad [5]$$

with n as the number density of the system.

Fig. 2 presents the temperature dependence of the dimensionless two-body entropy $s_2/k_{\rm B}$ for the different functionals, compared with FF results. We note that the $g(r)$ simulated with the TIP4P/2005 FF presents some discrepancies with respect to the experimental $g(r)$ at 300 K (66), mostly pertaining to the first peak, which is more pronounced compared to the experiment (78). However, the change of s_2 with temperature is in qualitative agreement with experiments for a wide range of temperatures, down to the supercooled regime (79).

One can observe that SCAN is the functional that best describes the s_2 temperature evolution, as compared to FF. Accounting for NQEs (see SCAN+NQE in Fig. 2) does not produce significant changes in the behavior of $s_2/k_{\rm B}$, even at the low temperature of 260 K. The optB88-vdW functional reproduces
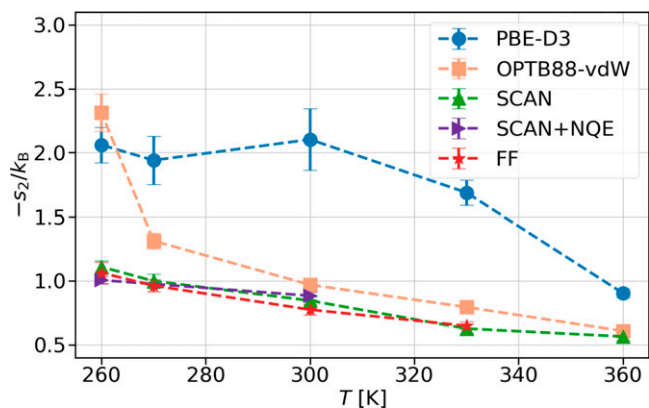

Fig. 2. Dimensionless two-body entropy $s_2/k_{\rm B}$ for different functionals and for FF as a function of the temperature.

the water structure—as represented by the s_2 order parameter—at the highest temperature of 360 K, but it gives rise to serious over structuring in the supercooled regime, thus leading to an overestimation of more than 2 times the value of s_2 at 260 K. Instead, PBE-D3 fails at recovering the liquid two-body entropy at any temperature, and the integral in Eq. **5** reaches a plateau for the lowest temperatures; that is, the $g(r)$ oscillations amplitude is not significantly affected by temperature, hinting at a possible glass transition (48).

To elucidate the connection between the water structure and the transport coefficients through the s_2 order parameter, we compare the radial distribution functions and the $s_2/k_{\rm B}$ running integrals for the FF and the SCAN functional at 260 K and at 300 K, both with classical and with quantum nuclei (Fig. 3); the comparison with the PBE-D3 and optB88-vdW functionals can be found in *SI Appendix*. At 300 K, the quantum nuclear $g(r)$ displays a lower first peak compared to the classical one

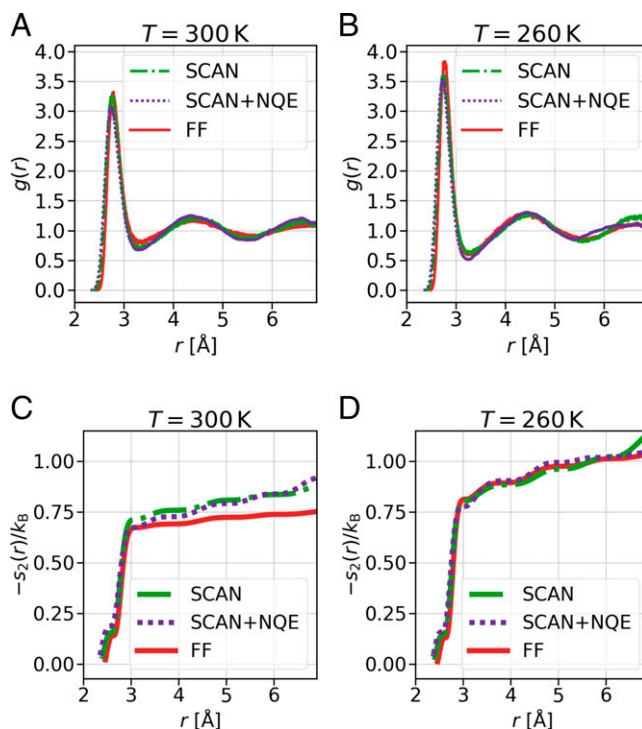**Fig. 3.** (*A* and *B*) Radial distribution functions and (*C* and *D*) $-s_2/k_{\rm B}$ running integrals of water at 300 and 260 K obtained from the SCAN functional with classical and quantum nuclei (SCAN+NQEs) as well as from the FF simulations.

and to the $g(r)$ from the FF, while the rise in the first peak also occurs at a slightly shorter distance. Thus, NQEs give rise to a less-structured first coordination shell, in qualitative agreement with experimental results in H_2O and D_2O which display these same characteristics (80). Although both the FF and SCAN overall predict a more pronounced first peak compared to experiments at 300 K (78), including NQEs with the SCAN functional partly improves upon the description of the first peak. Beyond the first peak, an increased structure is observed in the $g(r)$ predicted with SCAN+NQE, compared to the case with classical nuclei and with the FF result, in disagreement with experiments on light and heavy water (80). Such a discrepancy has been observed in previous PIMD simulations obtained with semilocal density functionals (12, 81), where it was pointed out that the origin of the increased structure of the second peak arises from the destabilization of interstitial hydrogen-bonded configurations occurring in quantum nuclear simulations, and more-accurate descriptions might alter this balance, thus leading to less-structured second and third solvation shells (16, 82). Shifting the focus to the s_2/k_B running integral (Fig. 3C), it can be noticed that, although the largest contribution to the limiting value of s_2/k_B arises from the first solvation shell, a nonnegligible part is also due to oscillations beyond the first solvation shell. Thus, as a result of a less-structured first solvation shell and of more-structured second and third shells, the SCAN+NQE functional predicts a limiting value of s_2/k_B that is similar to SCAN with classical nuclei, whereas the s_2/k_B value predicted with FF is visibly lower. Interestingly, the differences between the quantum and classical nuclear $g(r)$, observed at 300 K, are attenuated at 260 K, and also when comparing with the FF results. This leads to a value of s_2/k_B that is remarkably similar for all the three methods at 260 K, as seen in Fig. 3D.

Finally, in order to establish a relation between structure and transport coefficients, we proceed to test the entropy excess scaling laws. In that regard, it has been verified that the entropy excess s_{ex} can be approximated by the two-body contribution $s_{ex} \simeq s_2$ for water and supercooled binary mixtures (60–63). As described in ref. 83, s_2 is constructed from the oxygen–oxygen, oxygen–hydrogen, and hydrogen–hydrogen pair distributions. Still, the scaling laws hold well by just computing s_2 from the oxygen–oxygen $g(r)$, amounting to only considering the translational two-body entropy, with a difference of a factor of 3 between the estimates, so $s_{ex} \simeq 3s_2$ from our results. The dimensionless diffusion coefficient D/D_0 is expected to scale as (84) (*SI Appendix*)

$$\frac{D}{D_0} = A \exp(-B\, s_2/k_B), \qquad [6]$$

with $D_0 = l_0\sqrt{k_B T/m}$ (where $l_0 = n^{-1/3}$ is the average interparticle distance and m is the fluid mass), and A and B as dimensionless constants at a given fluid density. Considering this Eq. **6**, together with the SE equation, and assuming $R_h \approx l_0$, one can expect a scaling for the dimensionless viscosity η/η_0 as

$$\frac{\eta}{\eta_0} = A' \exp(-B'\, s_2/k_B), \qquad [7]$$

with $\eta_0 = \sqrt{mk_B T}/l_0^2$. From the SE relation, one expects $B' = -B$ and $A \cdot A' = l_0/(6\pi R_h)$.

We tested Eqs. **6** and **7** for the different functionals. Fig. 4 shows the results for the dimensionless transport coefficients as a function of the two-body entropy excess for the different functionals. One can see that, although the functionals predict different transport coefficients (Fig. 1) and s_2 results (Fig. 2), all of them verify an exponential scaling of η_{GK}/η_0 and D_{GK}/D_0
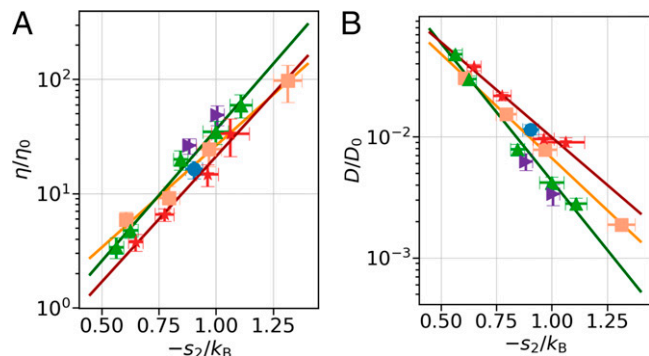

Fig. 4. Reduced (*A*) viscosity η/η_0 and (*B*) diffusion coefficient D/D_0, defined in Eqs. **6** and **7**, as a function of the dimensionless two-body entropy s_2/k_B for different functionals and FF simulations. The lines represent the respective exponential fits for each functional. The fit results are detailed in Table 1. The color and marker style representing the different functionals are the same as in Fig. 2.

with s_2. Therefore, we fitted the relations in Eqs. **6** and **7** for optB88-vdW, SCAN, and FF (continuous lines in Fig. 4). No fit was performed for PBE-D3, due to the single value measure we could report for this functional. The fit results are indicated in Table 1. One can observe that, although outside of the error bars, the fit parameters for SCAN and FF are the closest ones. Moreover, for all functionals, $B' = -B$ and $A \cdot A' = l_0/(6\pi R_h)$ with $l_0 \approx 2.8$ Å, implying a verification of the SE relation, Eq. **2**.

One can exploit the exponential relationship between the transport coefficients and s_2 to predict transport properties from structural ones: Once the fitting parameters in Eqs. **6** and **7** have been extracted by calculating the dependence of η and D on s_2 for a limited set of temperatures, the value of the transport coefficients can be obtained just from the calculation of the s_2 order parameter via the radial distribution function in a wider temperature range. Indeed, generally, structural properties such as the $g(r)$ require shorter simulations to converge, especially when using force-based methods, such as the one proposed in ref. 64, to reduce the variance when compared to the conventional strategies based on particle position binning. Fig. 5 presents the Green–Kubo results and their comparison with the prediction resulting from the fit via s_2. One can see good agreement between the explicit calculation of transport coefficients and their predictions via s_2 for all the data. Also, although the transport coefficients could not be calculated explicitly for the optB88-vdW functional at the lowest temperature of 260 K, they could be determined from the exponential relationship with s_2, yielding an exceedingly high viscosity and low diffusion, and thus verifying the failure of this functional in reproducing the temperature dependence of both transport coefficients.

Table 1. Fit parameters of the two-body excess entropy scaling relation for the dimensionless viscosity and diffusion coefficient, for different functionals and FF simulations

| | η_{GK}/η_0 | | D_{GK}/D_0 | |
	A' ($\times 10^{-1}$)	B'	A ($\times 10^{-1}$)	B
optB88-vdW	4.29(1.39)	4.11(0.34)	3.52(0.29)	−3.97(0.09)
SCAN	1.79(0.48)	5.31(0.31)	8.17(2.49)	−5.24(0.36)
FF	1.92(0.26)	4.52(0.18)	7.73(1.25)	−4.58(0.21)

The fit corresponds to the function $y = A \exp(-Bs_2/k_B)$ with y as the dimensionless viscosity η_{GK}/η_0, following Eq. **7**, and diffusion coefficient D_{GK}/D_0, following Eq. **6**.
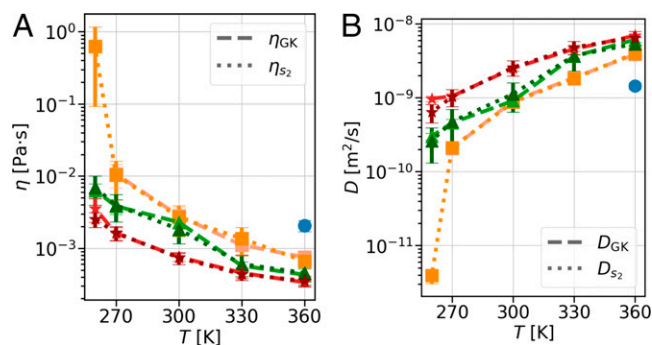
Fig. 5. Temperature evolution for different functionals of (*A*) shear viscosity from Eq. **7** and (*B*) diffusion coefficient from Eq. **6** with fit parameters from Table 1. A good agreement is found between the s_2-based prediction (dotted lines) and the explicit calculation (dashed lines), verifying the link between the structure and the transport coefficients. The color and marker style representing the different functionals are the same as in Fig. 1.

Conclusions

In summary, among the selected DFT functionals, SCAN best captures the temperature evolution of water transport properties—as described by the accurate TIP4P/2005 FF—despite the disagreement observed at temperatures of 300 K and below. We detected large discrepancies between functionals, with a major failure of PBE-D3, which is far too viscous. Despite these discrepancies, the SE relation was observed to hold in the considered temperature range for all the functionals, indicating that they all behave as (possibly supercooled) liquids, far enough from the glass transition that dynamical heterogeneities have not appeared yet (38, 77). Moreover, all of them predicted the same (no-slip) hydrodynamic radius $R_h \approx 1$ Å, corresponding to an effective hydrodynamic diameter of a slipping sphere of ~ 3 Å. This property, together with the finite-size correction for the diffusion coefficient, allowed us to propose a measure of viscosity η_{R_h} and diffusion coefficient D_{R_h}, based only on the slope of the mean-squared displacement in the diffusive regime D_{PBC}, for known box size and fixed R_h.

Motivated by a possible connection between dynamics and structure, we computed the radial distribution functions for the different functionals. Analogously to the transport coefficient results, we observed that SCAN radial distribution function is the one that better compares to FF, with little differences at the lowest temperatures in the second and third solvation shells, whereas PBE-D3 was far more structured that SCAN and optB88-vdW at high temperatures, in agreement with the high viscosity value measured for this functional. An explicit relationship between dynamics and structure can be established through the two-body entropy excess, which is an integral of a function of the radial distribution function. We verified the exponential relation on s_2 for both reduced bulk transport coefficients, and, although the connection between s_2 and transport properties is not univocal, as different fitting parameters were used for each functional, the fitting parameters all have the same order of magnitude. We suggest that the nonuniversality of the exponential relation is due to the use of the translational two-body excess entropy; a more universal relation could be observed by using the full two-body excess entropy, although the related structural features would be less easy to interpret.

Additionally, based on the established exponential relation between the bulk transport coefficients, we computed both viscosity and diffusion coefficient from the s_2 results and the fitting parameters. This allowed us to estimate transport coefficients

for functionals strongly structured (for instance, optB88-vdW at 260 K), which present such a high viscosity value that longer simulations are needed in order to observe a well-defined plateau in the Green–Kubo integral. Therefore, we propose here that, once the exponential dependence has been determined for a few temperatures, the viscosity and diffusion coefficient can be determined only from structural properties, which typically require shorter simulation times to converge (64). This can be a useful technique to apply in order to calculate transport coefficients for very viscous systems, where the associated time scales are far from the ones computationally reachable with AIMD simulations.

The connection between transport coefficients and the radial distribution function via the two-body entropy excess also establishes some guidelines to choose a functional for simulations of nanofluidic systems, where a functional which better reproduces water's structure will more likely reproduce its dynamical properties. The s_2 order parameter can also be employed as an instrumental tool to gauge the potential of DFT or of high-accuracy methods in describing dynamics without computing transport properties explicitly, where the comparison between different s_2 values becomes more straightforward than the comparison between two $g(r)$ profiles, or just the value of the $g(r)$ minimum or maximum, which does not ensure a full structure correlation. Indeed, from the $s_2(r)$ running integrals, we highlighted the importance of reproducing not only the first solvation shell of the $g(r)$ but also its long-range structure, which represents a nonnegligible contribution to the s_2 value. This feature, together with the scaling behavior of the bulk transport coefficients as a function of entropy, suggests that it is important that DFT reproduces not only the first peak in the $g(r)$ but also its long-range behavior, which is critical to obtain an accurate description of dynamical properties such as viscosity and diffusion coefficient.

Overall, among this large variety of results, we highlight two main messages. First, the SE relation is valid for all the functionals with, surprisingly, the same hydrodynamic radius of $\sim$1 Å, providing a way to predict the viscosity and self-diffusion coefficient from the slope of the mean-squared displacement in finite-size simulations. Second, the transport coefficients depend exponentially on the two-body excess entropy, a purely structural parameter, which hints at an underlying connection between structural and dynamical properties.

It is worth discussing the possible origins of the discrepancies of the temperature evolution of the viscosity and of the diffusion coefficient, particularly for the SCAN functional, which shows good agreement with FF and experiments at high temperatures but overestimates the viscosity and underestimates the diffusion coefficient at low temperatures. Although one might expect that the inclusion of zero-point energy and quantum tunneling, which become increasingly relevant at lower temperatures, would play an important role, we have shown that taking NQEs into account did not improve upon the results obtained with classical nuclei. As such, the most likely source of discrepancy lies in the approximate description of the electronic structure with the chosen functionals. Capturing the delicate balance between van der Waals dispersion and exchange interactions constitutes the main challenge for the description of water (10), and it is also critical in order to predict water transport properties below room temperature. From the limited selection of functionals chosen here, SCAN is the one that best describes the temperature evolution of the water viscosity and diffusion coefficient, even though other dispersion-corrected, semilocal, or hybrid functionals, such as revPBE-D3 (85, 86) and revPBE0-D3 (85–87), might present similar or even improved performance (16, 88, 89). Nevertheless, having determined that the SE relation and the exponential

scaling between D and s_2 and between η and s_2 hold for the TIP4P/2005 FF, the SCAN, and the optB88-vdW functionals suggests that both the validity of the SE relation and the scaling involving s_2 are not functional dependent. It remains to be seen whether the use of high-accuracy methods such as the random-phase approximation (RPA), Møller–Plesset perturbation theory (MP2) (11), and quantum Monte Carlo (90) would also improve upon the current description of water transport properties in supercooled conditions. Recent results on the diffusion coefficient for a wide range of temperatures obtained with RPA (91) and MP2 (92), also including the role of NQEs, are promising in this regard. As a further interesting perspective of this work, the established connection between the structure and dynamics might reveal what tips the balance between the strengthening and the weakening quantum delocalization effects of the H-bond network in water. Since diffusion is found, experimentally, to vary significantly between D_2O and H_2O (12), and s_2 is directly connected to diffusion, one can estimate the impact of the competing H-bond strengthening and weakening NQEs on the structure and the dynamics directly from the experimental measurements of the diffusivity and of the radial distribution function of light and heavy water at different temperatures. In that regard, it would be interesting to explore the contribution of the other $g(r)$ beyond the oxygen–oxygen one to the excess entropy, which could be more strongly impacted by isotopic effects. Finally, particularly intriguing questions pertain to the structure and dynamics of aqueous electrolytes (93), including what is the impact of structure-making and structure-breaking ions on the water $g(r)$ and on its diffusion coefficient (94, 95), of dynamical heterogeneity and how it may alter the SE relation (94), and of long-range intermolecular correlations and of NQEs on the viscosity of the solution (96, 97).

SI Appendix. *SI Appendix* provides computational details, derivation of excess entropy scaling relations, supporting figures, examples of input scripts, and data files for the simulations.

Materials and Methods

Simulation Details. We performed AIMD simulations of bulk water using DFT with the CP2K code (development version) (98), which employs the Gaussian and plane waves method to describe the wave function and the electron density and to solve the Kohn–Sham equations (99). Three different density functionals were considered: PBE (67) with Grimme's D3 corrections (68, 69), optB88-vdW (70, 71), and SCAN (72). The electronic structure problem was solved within the Born–Oppenheimer approximation for 5 different temperatures ($T = \{260, 270, 300, 330, 360\}$ K (the two lowest ones corresponding to the expected supercooled regime) controlled via the Nosé–Hoover thermostat. Most of the simulations were carried out with 32 water molecules (finite-size effects were taken into account as detailed in *SI Appendix*; in particular, we simulated 128 water molecules for SCAN at 330 and 270 K). We worked at constant volume with a box size such that $\rho = 1$ g/cm^3 ($L_{box} = 9.85$ Å for 32 water molecules). The running time was $\simeq 120$ ps for all functionals and temperatures except optB88-vdW and $T = \{260, 270\}$ K, with running time $\simeq 240$ ps. The time step considered was 0.5 fs. The initial configuration for all the functionals corresponded to the steady state at the given temperature obtained from FF MD after a running time of 200 ps. The energy cutoff for plane waves was 600 Ry for

PBE-D3 and optB88-vdW, and 800 Ry for SCAN, and the localized Gaussian basis set was short-range molecularly optimized double-ζ valence polarized (100).

NQEs were modeled using PIMD simulations with a thermostated ring polymer contraction scheme using 24 replicas (101, 102). PIMD simulations were performed using the i-PI code (103) together with CP2K, where the former is used to propagate the quantum nuclear dynamics, whereas the latter is used for the optimization of the wave function and to calculate the forces on each atom. Sampling in the canonical ensemble has been carried out at 260 and 300 K for 35 ps. Further, in the case of the PIMD simulations, the electronic structure problem is solved using subsystem DFT within the Kim–Gordon (KG) scheme, where the shortcomings of the electronic kinetic energy term of KG-DFT are addressed by correcting this term via a Δ-machine learning approach (104). Specifically, we use a neural network potential based on the Behler–Parrinello scheme (105) to learn the difference in the total energy and atomic forces between KS-DFT and KG-DFT (see ref. 73 and *SI Appendix* for further details). The resulting Δ-learning method provides the same accuracy as KS-DFT at the lower computational cost of KG-DFT.

We also performed FF (classical MD) simulations via the LAMMPS (large-scale atomic/molecular massively parallel simulator) package (106). Analogously to AIMD, we worked in the NVT ensemble with the temperature controlled via a Nosé–Hoover thermostat and with a volume such that $\rho = 1$ g/cm^3. Three different box sizes were considered: 32 water molecules ($L_{box} = 9.85$ Å), 64 water molecules ($L_{box} = 12.42$ Å), and 128 water molecules ($L_{box} = 15.64$ Å). The water model considered in all the cases was TIP4P/2005 (66).

Shear Viscosity and Diffusion Coefficient. For all the simulations, we determined the shear viscosity from the Green–Kubo relation,

$$\eta_{GK} = \frac{V}{k_B T} \int_0^\infty \langle p_{ij}(t) p_{ij}(0) \rangle dt, \qquad [8]$$

with V as the volume, k_B as the Boltzmann constant, T as the temperature, and $p_{ij} = \{p_{xy}, p_{xz}, p_{yz}\}$ as the nondiagonal components of the stress tensor.

The error bars were computed within 60% of confidence level. For viscosity, the total MD stress was divided into three time slots of equal length, each of them containing three independent measures of η. η_{GK} was measured at the time when the $\eta(t)$ running integral reached a time plateau (*SI Appendix*). Therefore, nine independent viscosity values were computed for each functional at a given temperature. For the diffusion coefficient, the first 20 ps were removed from the trajectory so the system equilibration from the initial configuration would not affect the mean-squared displacement results. From them, three independent measures of D_{PBC} were obtained from the three independent Cartesian components.

1. P. Gallo *et al.*, Water: A tale of two liquids. *Chem. Rev.* **116**, 7463–7500 (2016).
2. F. H. Stillinger, Water revisited. *Science* **209**, 451–457 (1980).
3. T. Morawietz, A. Singraber, C. Dellago, J. Behler, How van der Waals interactions determine the unique properties of water. *Proc. Natl. Acad. Sci. U.S.A.* **113**, 8368–8373 (2016).
4. H. S. Lee, M. E. Tuckerman, Structure of liquid water at ambient temperature from ab initio molecular dynamics performed in the complete basis set limit. *J. Chem. Phys.* **125**, 154507 (2006).
5. G. Cicero, J. C. Grossman, E. Schwegler, F. Gygi, G. Galli, Water confined in nanotubes and between graphene sheets: A first principle study. *J. Am. Chem. Soc.* **130**, 1871–1878 (2008).
6. O. Wohlfahrt, C. Dellago, M. Sega, Ab initio structure and thermodynamics of the RPBE-D3 water/vapor interface by neural-network molecular dynamics. *J. Chem. Phys.* **153**, 144710 (2020).
7. Z. Ye, A. Prominski, B. Tian, G. Galli, Probing the electronic properties of the electrified silicon/water interface by combining simulations and experiments. *Proc. Natl. Acad. Sci. U.S.A.* **118**, e2114929118 (2021).
8. T. E. Gartner III *et al.*, Signatures of a liquid-liquid transition in an ab initio deep neural network model for water. *Proc. Natl. Acad. Sci. U.S.A.* **117**, 26040–26046 (2020).

9. A. Bankura, A. Karmakar, V. Carnevale, A. Chandra, M. L. Klein, Structure, dynamics, and spectral diffusion of water from first-principles molecular dynamics. *J. Phys. Chem. C* **118**, 29401–29411 (2014).

10. M. J. Gillan, D. Alfè, A. Michaelides, Perspective: How good is DFT for water? *J. Chem. Phys.* **144**, 130901 (2016).

11. M. Del Ben, J. Hutter, J. VandeVondele, Probing the structural and dynamical properties of liquid water with models including non-local electron correlation. *J. Chem. Phys.* **143**, 054506 (2015).

12. M. Ceriotti *et al.*, Nuclear quantum effects in water and aqueous systems: Experiment, theory, and current challenges. *Chem. Rev.* **116**, 7529–7550 (2016).

13. O. Marsalek, T. E. Markland, Quantum dynamics and spectroscopy of ab initio liquid water: The interplay of nuclear and electronic quantum effects. *J. Phys. Chem. Lett.* **8**, 1545–1551 (2017).

14. M. Rossi, V. Kapil, M. Ceriotti, Fine tuning classical and quantum molecular dynamics using a generalized Langevin equation. *J. Chem. Phys.* **148**, 102301 (2018).

15. M. Ceriotti, G. Bussi, M. Parrinello, Nuclear quantum effects in solids using a colored-noise thermostat. *Phys. Rev. Lett.* **103**, 030603 (2009).

16. B. Cheng, E. A. Engel, J. Behler, C. Dellago, M. Ceriotti, Ab initio thermodynamics of liquid and solid water. *Proc. Natl. Acad. Sci. U.S.A.* **116**, 1110–1115 (2019).

17. A. Reinhardt, B. Cheng, Quantum-mechanical exploration of the phase diagram of water. *Nat. Commun.* **12**, 588 (2021).

18. T. D. Kühne, M. Krack, M. Parrinello, Static and dynamical properties of liquid water from first principles by a novel Car–Parrinello-like approach. *J. Chem. Theory Comput.* **5**, 235–241 (2009).

19. M. Chen *et al.*, Ab initio theory and modeling of water. *Proc. Natl. Acad. Sci. U.S.A.* **114**, 10846–10851 (2017).

20. H. S. Lee, M. E. Tuckerman, Dynamical properties of liquid water from ab initio molecular dynamics performed in the complete basis set limit. *J. Chem. Phys.* **126**, 164501 (2007).

21. S. Balasubramanian, C. J. Mundy, M. L. Klein, Shear viscosity of polar fluids: Molecular dynamics calculations of water. *J. Chem. Phys.* **105**, 11190–11195 (1996).

22. A. P. Markesteijn, R. Hartkamp, S. Luding, J. Westerweel, A comparison of the value of viscosity for several water models using Poiseuille flow in a nano-channel. *J. Chem. Phys.* **136**, 134104 (2012).

23. E. Guillaud, S. Merabia, D. de Ligny, L. Joly, Decoupling of viscosity and relaxation processes in supercooled water: A molecular dynamics study with the TIP4P/2005f model. *Phys. Chem. Chem. Phys.* **19**, 2124–2130 (2017).

24. T. Kawasaki, K. Kim, Identifying time scales for violation/preservation of Stokes-Einstein relation in supercooled water. *Sci. Adv.* **3**, e1700399 (2017).

25. P. Montero de Hijes, E. Sanz, L. Joly, C. Valeriani, F. Caupin, Viscosity and self-diffusion of supercooled and stretched water from molecular dynamics simulations. *J. Chem. Phys.* **149**, 094503 (2018).

26. R. Shi, J. Russo, H. Tanaka, Common microscopic structural origin for water's thermodynamic and dynamic anomalies. *J. Chem. Phys.* **149**, 224502 (2018).

27. I. N. Tsimpanogiannis *et al.*, Self-diffusion coefficient of bulk and confined water: A critical review of classical molecular simulation studies. *Mol. Simul.* **45**, 425–453 (2019).

28. T. I. Morozova, N. A. García, J. L. Barrat, Temperature dependence of thermodynamic, dynamical, and dielectric properties of water models. *J. Chem. Phys.* **156**, 126101 (2022).

29. D. Alfè, M. J. Gillan, First-principles calculation of transport coefficients. *Phys. Rev. Lett.* **81**, 5161–5164 (1998).

30. C. Malosso, L. Zhang, R. Car, S. Baroni, D. Tisi, Viscosity in water from first-principles and deep-neural-network simulations. arXiv [Preprint] (2022). https://doi.org/10.48550/arXiv.2203.01262 (Accessed 4 March 2022).

31. P. Gallo, F. Sciortino, P. Tartaglia, S. Chen, Slow dynamics of water molecules in supercooled states. *Phys. Rev. Lett.* **76**, 2730–2733 (1996).

32. P. G. Debenedetti, Supercooled and glassy water. *J. Phys. Condens. Matter* **15**, R1669 (2003).

33. J. C. F. Schulz, A. Schlaich, M. Heyden, R. R. Netz, J. Kappler, Molecular interpretation of the non-Newtonian viscoelastic behavior of liquid water at high frequencies. *Phys. Rev. Fluids* **5**, 103301 (2020).

34. I. de Almeida Ribeiro, M. de Koning, Non-Newtonian flow effects in supercooled water. *Phys. Rev. Res.* **2**, 022004 (2020).

35. T. J. O'Sullivan, S. K. Kannam, D. Chakraborty, B. D. Todd, J. E. Sader, Viscoelasticity of liquid water investigated using molecular dynamics simulations. *Phys. Rev. Fluids* **4**, 123302 (2019).

36. Y. Jung, J. P. Garrahan, D. Chandler, Excitation lines and the breakdown of Stokes-Einstein relations in supercooled liquids. *Phys. Rev. E Stat. Nonlin. Soft Matter Phys.* **69**, 061205 (2004).

37. S. H. Chen *et al.*, The violation of the Stokes-Einstein relation in supercooled water. *Proc. Natl. Acad. Sci. U.S.A.* **103**, 12974–12978 (2006).

38. P. Kumar *et al.*, Relation between the Widom line and the breakdown of the Stokes-Einstein relation in supercooled water. *Proc. Natl. Acad. Sci. U.S.A.* **104**, 9575–9579 (2007).

39. L. Xu *et al.*, Appearance of a fractional Stokes–Einstein relation in water and a structural interpretation of its onset. *Nat. Phys.* **5**, 565–569 (2009).

40. Z. Shi, P. G. Debenedetti, F. H. Stillinger, Relaxation processes in liquids: Variations on a theme by Stokes and Einstein. *J. Chem. Phys.* **138**, 12A526 (2013).

41. L. Bocquet, E. Charlaix, Nanofluidics, from bulk to interfaces. *Chem. Soc. Rev.* **39**, 1073–1095 (2010).

42. A. Botan, B. Rotenberg, V. Marry, P. Turq, B. Noetinger, Hydrodynamics in clay nanopores. *J. Phys. Chem. C* **115**, 16109–16115 (2011).

43. B. Cross *et al.*, Wall slip of complex fluids: Interfacial friction versus slip length. *Phys. Rev. Fluids* **3**, 062001 (2018).

44. G. Tocci, M. Bilichenko, L. Joly, M. Iannuzzi, Ab initio nanofluidics: Disentangling the role of the energy landscape and of density correlations on liquid/solid friction. *Nanoscale* **12**, 10994–11000 (2020).

45. C. Herrero, G. Tocci, S. Merabia, L. Joly, Fast increase of nanofluidic slip in supercooled water: The key role of dynamics. *Nanoscale* **12**, 20396–20403 (2020).

46. M. H. Cohen, D. Turnbull, Molecular transport in liquids and glasses. *J. Chem. Phys.* **31**, 1164–1169 (1959).

47. D. Turnbull, M. H. Cohen, Free-volume model of the amorphous phase: Glass transition. *J. Chem. Phys.* **34**, 120–125 (1961).

48. M. I. Ojovan, D. V. Louzguine-Luzgin, Revealing structural changes at glass transition via radial distribution functions. *J. Phys. Chem. B* **124**, 3186–3194 (2020).

49. J. Russo, H. Tanaka, Understanding water's anomalies with locally favoured structures. *Nat. Commun.* **5**, 3556 (2014).

50. R. Shi, J. Russo, H. Tanaka, Origin of the emergent fragile-to-strong transition in supercooled water. *Proc. Natl. Acad. Sci. U.S.A.* **115**, 9444–9449 (2018).

51. H. Tong, H. Tanaka, Structural order as a genuine control parameter of dynamics in simple glass formers. *Nat. Commun.* **10**, 5596 (2019).

52. M. C. Gao, M. Widom, Information entropy of liquid metals. *J. Phys. Chem. B* **122**, 3550–3555 (2018).

53. C. Zhang, L. Spanu, G. Galli, Entropy of liquid water from ab initio molecular dynamics. *J. Phys. Chem. B* **115**, 14190–14195 (2011).

54. M. Dzugutov, A universal scaling law for atomic diffusion in condensed matter. *Nature* **381**, 137–139 (1996).

55. I. Yokoyama, A relationship between excess entropy and diffusion coefficient for liquid metals near the melting point. *Physica B* **254**, 172–177 (1998).

56. T. S. Ingebrigtsen, H. Tanaka, Structural predictor for nonlinear sheared dynamics in simple glass-forming liquids. *Proc. Natl. Acad. Sci. U.S.A.* **115**, 87–92 (2018).

57. A. Baranyai, D. J. Evans, Direct entropy calculation from computer simulation of liquids. *J. Non-Cryst. Solids* **117–118**, 593–596 (1990).

58. Y. D. Fomin, V. N. Ryzhov, B. A. Klumov, E. N. Tsiok, How to quantify structural anomalies in fluids? *J. Chem. Phys.* **141**, 034508 (2014).

59. M. K. Nandi, A. Banerjee, S. Sengupta, S. Sastry, S. M. Bhattacharyya, Unraveling the success and failure of mode coupling theory from consideration of entropy. *J. Chem. Phys.* **143**, 174504 (2015).

60. J. Mittal, J. R. Errington, T. M. Truskett, Quantitative link between single-particle dynamics and static structure of supercooled liquids. *J. Phys. Chem. B* **110**, 18147–18150 (2006).

61. J. Mittal, J. R. Errington, T. M. Truskett, Relationships between self-diffusivity, packing fraction, and excess entropy in simple bulk and confined fluids. *J. Phys. Chem. B* **111**, 10054–10063 (2007).

62. R. Chopra, T. M. Truskett, J. R. Errington, On the use of excess entropy scaling to describe single-molecule and collective dynamic properties of hydrocarbon isomer fluids. *J. Phys. Chem. B* **114**, 16487–16493 (2010).

63. I. H. Bell, J. C. Dyre, T. S. Ingebrigtsen, Excess-entropy scaling in supercooled binary mixtures. *Nat. Commun.* **11**, 4300 (2020).

64. B. Rotenberg, Use the force! Reduced variance estimators for densities, radial distribution functions, and local mobilities in molecular simulations. *J. Chem. Phys.* **153**, 150902 (2020).

65. L. Zheng *et al.*, Structural, electronic, and dynamical properties of liquid water by ab initio molecular dynamics based on SCAN functional within the canonical ensemble. *J. Chem. Phys.* **148**, 164505 (2018).

66. J. L. Abascal, C. Vega, A general purpose model for the condensed phases of water: TIP4P/2005. *J. Chem. Phys.* **123**, 234505 (2005).

67. J. P. Perdew, K. Burke, M. Ernzerhof, Generalized gradient approximation made simple. *Phys. Rev. Lett.* **77**, 3865–3868 (1996).

68. S. Grimme, Accurate description of van der Waals complexes by density functional theory including empirical corrections. *J. Comput. Chem.* **25**, 1463–1473 (2004).

69. S. Grimme, Semiempirical GGA-type density functional constructed with a long-range dispersion correction. *J. Comput. Chem.* **27**, 1787–1799 (2006).

70. J. Klimeš, D. R. Bowler, A. Michaelides, Chemical accuracy for the van der Waals density functional. *J. Phys. Condens. Matter* **22**, 022201 (2010).

71. J. Klimeš, D. R. Bowler, A. Michaelides, Van der Waals density functionals applied to solids. *Phys. Rev. B Condens. Matter Mater. Phys.* **83**, 195131 (2011).

72. J. Sun, A. Ruzsinszky, J. P. Perdew, Strongly constrained and appropriately normed semilocal density functional. *Phys. Rev. Lett.* **115**, 036402 (2015).

73. M. Pauletti, V. V. Rybkin, M. Iannuzzi, Subsystem density functional theory augmented by a delta learning approach to achieve Kohn–Sham accuracy. *J. Chem. Theory Comput.* **17**, 6423–6431 (2021).

74. S. Tazi *et al.*, Diffusion coefficient and shear viscosity of rigid water models. *J. Phys. Condens. Matter* **24**, 284117 (2012).

75. I. C. Yeh, G. Hummer, System-size dependence of diffusion coefficients and viscosities from molecular dynamics simulations with periodic boundary conditions. *J. Phys. Chem. B* **108**, 15873–15879 (2004).

76. L. B. Weiss, V. Dahirel, V. Marry, M. Jardat, Computation of the hydrodynamic radius of charged nanoparticles from nonequilibrium molecular dynamics. *J. Phys. Chem. B* **122**, 5940–5950 (2018).

77. M. G. Mazza, N. Giovambattista, H. E. Stanley, F. W. Starr, Connection of translational and rotational dynamical heterogeneities with the breakdown of the Stokes-Einstein and Stokes-Einstein-Debye relations in water. *Phys. Rev. E Stat. Nonlin. Soft Matter Phys.* **76**, 031203 (2007).

78. L. B. Skinner *et al.*, Benchmark oxygen-oxygen pair-distribution function of ambient water from x-ray diffraction measurements with a wide Q-range. *J. Chem. Phys.* **138**, 074506 (2013).

79. G. Camisasca, H. Pathak, K. T. Wikfeldt, L. G. M. Pettersson, Radial distribution functions of water: Models vs experiments. *J. Chem. Phys.* **151**, 044502 (2019).

80. A. K. Soper, C. J. Benmore, Quantum differences between heavy and light water. *Phys. Rev. Lett.* **101**, 065502 (2008).

81. P. Gasparotto, A. A. Hassanali, M. Ceriotti, Probing defects and correlations in the hydrogen-bond network of ab initio water. *J. Chem. Theory Comput.* **12**, 1953–1964 (2016).

82. M. Del Ben, J. Hutter, J. VandeVondele, Probing the structural and dynamical properties of liquid water with models including non-local electron correlation. *J. Chem. Phys.* **143**, 054506 (2015).

83. M. Agarwal, M. P. Alam, C. Chakravarty, Thermodynamic, diffusional, and structural anomalies in rigid-body water models. *J. Phys. Chem. B* **115**, 6935–6945 (2011).

84. J. C. Dyre, Perspective: Excess-entropy scaling. *J. Chem. Phys.* **149**, 210901 (2018).

85. Y. Zhang, W. Yang, Comment on "Generalized gradient approximation made simple." *Phys. Rev. Lett.* **80**, 890 (1998).

86. L. Goerigk, S. Grimme, A thorough benchmark of density functional methods for general main group thermochemistry, kinetics, and noncovalent interactions. *Phys. Chem. Chem. Phys.* **13**, 6670–6688 (2011).

87. C. Adamo, V. Barone, Toward reliable density functional methods without adjustable parameters: The pbe0 model. *J. Chem. Phys.* **110**, 6158–6170 (1999).

88. M. Galib *et al.*, Mass density fluctuations in quantum and classical descriptions of liquid water. *J. Chem. Phys.* **146**, 244501 (2017).

89. L. Ruiz Pestana, N. Mardirossian, M. Head-Gordon, T. Head-Gordon, *Ab initio* molecular dynamics simulations of liquid water using high quality meta-GGA functionals. *Chem. Sci. (Camb.)* **8**, 3554–3565 (2017).

90. A. Zen, Y. Luo, G. Mazzola, L. Guidoni, S. Sorella, Ab initio molecular dynamics simulation of liquid water by quantum Monte Carlo. *J. Chem. Phys.* **142**, 144111 (2015).

91. Y. Yao, Y. Kanai, Nuclear quantum effect and its temperature dependence in liquid water from random phase approximation via artificial neural network. *J. Phys. Chem. Lett.* **12**, 6354–6362 (2021).

92. J. Lan, D. Wilkins, V. Rybkin, M. Iannuzzi, J. Hutter, Quantum dynamics of water from Møller-Plesset perturbation theory via a neural network potential. ChemRxiv [Preprint] (2021). https://doi.org/10.26434/chemrxiv-2021-n32q8-v2 (Accessed 10 May 2022).

93. T. T. Duignan *et al.*, Quantifying the hydration structure of sodium and potassium ions: Taking additional steps on Jacob's Ladder. *Phys. Chem. Chem. Phys.* **22**, 10641–10652 (2020).

94. Y. Ding, A. A. Hassanali, M. Parrinello, Anomalous water diffusion in salt solutions. *Proc. Natl. Acad. Sci. U.S.A.* **111**, 3310–3315 (2014).

95. A. P. Gaiduk, G. Galli, Local and global effects of dissolved sodium chloride on the structure of water. *J. Phys. Chem. Lett.* **8**, 1496–1502 (2017).

96. Y. Chen *et al.*, Electrolytes induce long-range orientational order and free energy changes in the H-bond network of bulk water. *Sci. Adv.* **2**, e1501891 (2016).

97. J. Dedic, H. I. Okur, S. Roke, Polyelectrolytes induce water-water correlations that result in dramatic viscosity changes and nuclear quantum effects. *Sci. Adv.* **5**, eaay1443 (2019).

98. T. D. Kühne *et al.*, CP2K: An electronic structure and molecular dynamics software package–Quickstep: Efficient and accurate electronic structure calculations. *J. Chem. Phys.* **152**, 194103 (2020).

99. J. VandeVondele *et al.*, Quickstep: Fast and accurate density functional calculations using a mixed Gaussian and plane waves approach. *Comput. Phys. Commun.* **167**, 103–128 (2005).

100. J. VandeVondele, J. Hutter, Gaussian basis sets for accurate calculations on molecular systems in gas and condensed phases. *J. Chem. Phys.* **127**, 114105 (2007).

101. I. R. Craig, D. E. Manolopoulos, Quantum statistics and classical mechanics: Real time correlation functions from ring polymer molecular dynamics. *J. Chem. Phys.* **121**, 3368–3373 (2004).

102. S. Habershon, D. E. Manolopoulos, T. E. Markland, T. F. Miller 3rd, Ring-polymer molecular dynamics: Quantum effects in chemical dynamics from classical trajectories in an extended phase space. *Annu. Rev. Phys. Chem.* **64**, 387–413 (2013).

103. V. Kapil *et al.*, i-pi 2.0: A universal force engine for advanced molecular simulations. *Comput. Phys. Commun.* **236**, 214–223 (2019).

104. R. Ramakrishnan, P. O. Dral, M. Rupp, O. A. von Lilienfeld, Big data meets quantum chemistry approximations: The δ-machine learning approach. *J. Chem. Theory Comput.* **11**, 2087–2096 (2015).

105. J. Behler, M. Parrinello, Generalized neural-network representation of high-dimensional potential-energy surfaces. *Phys. Rev. Lett.* **98**, 146401 (2007).

106. A. P. Thompson *et al.*, LAMMPS–A flexible simulation tool for particle-based materials modeling at the atomic, meso, and continuum scales. *Comput. Phys. Commun.* **271**, 108171 (2022).

107. C. Herrero, M. Pauletti, G. Tocci, M. Iannuzzi, L. Joly, Connection between water's dynamical and structural properties: Insights from ab initio simulations. Zenodo. https://doi.org/10.5281/zenodo.6458419. Deposited 13 April 2022.